Ab Initio Study of Dehydroxylation−Carbonation Reaction on Brucite Surface

Sergey V. Churakov,* Marchella Iannuzzi, and Michele Parrinello

Laboratory of Physical Chemistry, ETH Zurich, USI Campus, Via Giuseppe Buffi 13, CH-6904 Lugano, Switzerland

Received: December 19, 2003; In Final Form: March 1, 2004

The possibility of forming magnesite from brucite crystallites, in a CO_2-rich environment, has attracted large interest as a possible industrial procedure to store CO_2 in the form of carbonate minerals. The reaction mechanisms responsible for such processes are, however, not very well-known. In this work we first consider the compatibility of the magnesite and brucite structures, along specific crystallographic directions. In the second part we describe the sequence of events that leads to the formation of a magnesite layer, via the dehydroxylation of brucite and consequent adsorption and diffusion of carbon complexes. To observe these thermally activated events, we employ a method recently developed in our group[1,2] for finding complex reaction pathways and reproducing the related free energy surface. We find that the $(1\bar{1}00)$ brucite surface can be dehydroxylated quite easily. The formation of vacancies in the hydroxyl layers might favor the diffusion of OH and protons through the channels between two neighboring (0001) OH planes, which characterize the brucite structure. This mechanism creates the necessary conditions for further dehydroxylation and formation of magnesite layers.

Introduction

The problem of global warming caused by the explosive growth of CO_2 pollution calls for new and efficient ways to eliminate the carbon dioxide. Taking a cue from the processes of chemical weathering on the Earth's surface, it has been suggested that industrially produced CO_2 could be stored in the form of carbonate minerals.[3] This could occur as the result of the reaction of carbon dioxide with silicate, hydroxides, or oxide of alkali earth metals.[4] The keys to success for this project will be the efficiency and low cost of CO_2 sequestration.

Chemically and structurally simple minerals, such as $Mg(OH)_2$ (brucite), are commonly used in experimental and theoretical research to better understand the sequestration problem. Although the dehydroxylation process

$$Mg(OH) \rightleftharpoons MgO + H_2O \tag{1}$$

has been extensively studied, very little is known at the atomic level. Experimentally, the equilibrium of this reaction is a strong function of vapor pressure. For example, at 1 bar the decomposition of the structure starts at 545 K, whereas at 500 bar brucite is stable up to 840 K. The activation barrier characterizing the reaction has been estimated between 13 and 58 kcal/mol.[5−8] During dehydroxylation at relatively low temperatures, the lamellar brucite structure undergoes a variety of complex physical transformations, including translamellar creaking, delamination, and morphological reconstructions. As a result, highly reactive nanocrystals are formed.[6] High-resolution transition electron microscopy shows that during the dehydroxylation reaction a lamellar MgO structure can grow at the expense of the parent hydroxyl layers. As a result, a layered nMgO × mMg(OH)$_2$ solid solution is formed.[7] The thermodynamic stability and structural morphology of such a solid solution suggest that it can be formed by the interlamellar dehydroxylation of brucite, driven by interlayer diffusion.[7,9]

The main focus of this work is the study of the dehydroxylation/carbonation reaction

$$Mg(OH)_2 + CO_2 \rightleftharpoons MgCO_3 + H_2O \tag{2}$$

which is a complex process requiring the simultaneous advance of reaction 1 and of the carbonation of MgO

$$MgO + CO_2 \rightleftharpoons MgCO_3 \tag{3}$$

Although the rate of the dehydroxylation increases with temperature, the carbonation is limited by the temperature stability of magnesium carbonate (magnesite). On the other hand, even if the carbonation process is most efficient just above critical carbonation pressure,[6] the global reaction rate decreases at higher CO_2 pressure, since the activation barrier for dehydroxylation increases up to 80 kcal/mol. The common interpretation of this effect is that a carbonate layer is formed on the partially dehydroxylated surface preventing the further release of OH.[5,6] The formation of this first carbonate layer might also be the precursor step for further growth of a magnesium carbonate crystal by diffusion of carbon atoms in the bulk brucite, probably through the same channel used by OH and water molecules to reach the surface. Many experimental and theoretical studies suggest that the growth of magnesium carbonate takes place on the $(10\bar{1}4)$ cleavage plane.[10] However, the growth process has not yet been observed experimentally, and the details of the mechanism are not known.

These processes occur at the exposed surface of the particles of $Mg(OH)_2$ and are believed to be sustained first by the diffusion of H atoms and hydroxyl groups, and later of the C atoms, through the brucite crystal. Thus, the OH vacant sites, which are created in the bulk, can be occupied by the C atoms, and the carbonation can penetrate deep into the sample. The

* Corresponding author. Current address: Waste Management Laboratory, Paul Scherrer Institut, CH-5232 Villigen PSI, Switzerland. Tel: +41 056 310 4113. Fax: +41 056 310 2821. E-mail: sergey.churakov@psi.ch.

10.1021/jp037935x CCC: $27.50
Published on Web 07/09/2004

layered structure of brucite, indeed, provides wide, two-dimensional channels, whose walls are the (0001) hydroxyl layers and run along the $(1\bar{1}00)$ axis.

To understand better the simultaneous dehydroxylation/carbonation reaction, we use Car−Parrinello molecular dynamics (MD)[11] which has proven to be a powerful tool in describing complex processes in condensed phases. However, because of the high energy barriers characterizing these reactions, a standard MD run would require an unfeasibly long simulation time to reproduce such rare events. We have, therefore, resorted to a newly developed method, which allows the efficient study of rare events[1,2] and the estimation of the related free energy profile. With this method we are able to determine the microscopic details of dehydroxylation and carbonation of partly dehydroxylated surfaces in a few picoseconds of simulation time.

The article is organized as follows. First we provide some more computational details about the methodology we use in our study. Next we discuss the choice of the (1100) crystallographic plane as the surface where most likely the reactions take place. The main part of the results section is devoted to the metadynamics simulations and the analysis of the possible reaction pathways. Because of the complexity of the mechanism, which goes through many intermediate states, the dehydroxylation and the carbonation are taken into account separately.

Eventually we are able to estimate the energy barriers characterizing the different steps of the process and to address the probable pathways to the formation of the first magnesite layer from a brucite substrate.

Method

For all the calculations presented in this work, we use density functional theory[12] (DFT) in the generalized gradient approximation BLYP for the exchange-correlation functional.[13] The wave functions of the valence electrons are expanded into a plane-wave basis set, with 70 Ry energy cutoff. The interactions of the valence electrons with the cores are described by the pseudopotential (PP) formalism. We use fully separable, norm-conserving Troullier−Martins PP.[14] The nonlinear core correction is added for the Mg element in order to account for the significant overlap between its core and valence orbitals. Similar choices for the exchange-correlation functional, plane-wave cutoff, and PP have already been used successfully to study the bulk properties and the surface relaxation of brucite.[15,16] The ab initio Car−Parrinello MD simulations are performed,[11] with time step 0.15 fs and fictious electron mass 800 au.

Since in our applications the differences in the chemical behavior of H and deuterium are negligible, we always use the heavier D atoms, for the sake of a slightly longer integration time step.

To model a semiinfinite bulk system with an exposed surface, we use a 3D, periodically repeated box containing a slab of several atomic layers. Above the slab, we add at least 6 Å of empty space to reduce the interaction between periodic images. The surface energy calculations and the optimization of the ionic positions are performed with slabs of four layers, where the cell's side lengths are constrained at the experimental values and the surface is given by six (3×2) $Mg(OH)_2$ structural elements. The MD simulations, on the other hand, are performed by using slabs containing only two layers, but with larger surface areas $(3 \times 3\ Mg(OH)_2)$. The larger surface area is required in order to avoid spurious interactions of the reaction products with their periodic images. The atoms in the bottom layer of the slab are kept fixed to maintain the equilibrium configuration of the bulk. By this trick, we are able to model the interaction of the surface with a rigid bulk system. The thinner slab can be safely used because there are no important interactions between the surface and the layers which are deeper; therefore, this choice does not affect the reaction process.

The long time scales required to observe thermally activated processes, such as the brucite dehydroxylation and carbonation reactions, are not accessible to standard MD techniques. Recently, in our group, a new method has been developed that is able to deal with this kind of problem.[1,2] The method, known as metadynamics, is based on the coarse-grained representation of the system, in terms of a few collective variables (CV), and on the construction of a metadynamics trajectory in the configuration space defined by these CV.

The CV are analytic functions of the of the ionic positions, $S(\{R_I\})$. The correct reactive path can be reproduced if the CV are able to distinguish among reactants, products, and all the intermediates visited along the transformation path. In addition, it is important that the relevant modes, which need to be activated in the process, can be represented in the CV space. The metadynamics trajectory is derived from the non-Markovian, extended Lagrangian, as described in ref 2.

$$L = L_{CP} + \sum_a \frac{1}{2} M_a \dot{s}_a^2 - \sum_a \frac{1}{2} k_a (S_a(\{R_I\}) - s_a)^2 + V(t,\{s_a\}) \quad (4)$$

where L_{CP} is the standard Car−Parrinello Lagrangian.[11] For each selected $S_a(\{R_I\})$, an additional dynamic variable s_a is introduced. The $\{s_a\}$ are coupled to the microscopic system via the harmonic potential $^1/_2 k_a (S_a(\{R_I\}) - s_a)^2$. The time-dependent potential $V(t,\{s_a\})$ is introduced to enhance the sampling of the configurational space. $V(t,\{s_a\})$ is constructed as a sum of repulsive, hill-like potentials that discourage the system from returning into previously explored configurations. This pushes the system in new states over the lowest energy barriers, thus preventing it from being trapped in local minima. It has been shown in ref 2 that if the values of M_a and k_a are chosen so that dynamics of the $\{s_a\}$ is adiabatically decoupled from the faster ionic and electronic motion, the $V(t,\{s_a\})_{t\to\infty} = F(\{s_a\})$ within a constant. The free energy surface is defined by

$$F(\{s_a\}) = -k_B T \ln \int dR\, \delta(\{S_a(R)\} - \{s_a\}) e^{-\beta V(R)} \quad (5)$$

where $V(R)$ is the interaction potential. In the limit of infinite masses for the CV, the algorithm resembles $\{s_a\}$ to the constraint molecular dynamics method, as introduced by Carter et al.[17] However, thanks to the on the fly update of the boosting potential and to the dynamic character of the CV, our method is more efficient in sampling a multidimensional configuration space. Moreover, the metadynamics generates trajectories, which lay on the minimum-energy path and provide a better understanding of the reaction process.

The accuracy of the evaluation of the free energy profile depends on the size of the hill-like contributions that build up the time-dependent potential. The larger those contributions, the faster the system move to new configurations in the CV space. However, this takes place at the cost of a proportional loss of resolution. Simulations on model systems[1,2] have shown that, for a sufficiently low accumulation rate of the hills, the achieved accuracy in the resolution of the free energy differences is exactly given by the hill height. In general, the used accumulation rate is somewhat faster to be efficient in sampling the free energy surface and to be accurate within few kcal mol^{-1}. By

placing one hill of about 0.5 kcal mol^{-1} every 75 fs, we get accuracy, which is about 1 order of magnitude larger than the hill height.

The method has been applied to several problems (conformation rearrangements, chemical reactivity, solid-phase transformations, etc.), and has proved to be efficient and reliable.[2,18] If the selected CV are general enough and do not bias the pathway in a specific direction, the method can also disclose unforeseen reaction mechanisms and predict unknown intermediate and final product states. In the application to the dehydration and the carbonation problems, we use as CV the coordination numbers of certain atoms or species to describe the formation or dissociation of the bonds. The coordination number (CN) of the atom I with respect to the subset of atoms j, where $j = 1$,.., N_J, is defined

$$\mathrm{CN}_I = \sum_{j=1}^{N_J} \frac{1 - \left(\frac{R_{Ij}}{R_0}\right)^6}{1 - \left(\frac{R_{Ij}}{R_0}\right)^{12}}$$

R_{Ij} is the interatomic distance and R_0 is the reference bond length. The terms in the sum move quickly to zero when the two atoms are farther than the reference value R_0, and the decay is determined by the exponents. If N_J is 1, CN is the reciprocal coordination between two specific atoms, and it is used like a switching function to determine the presence of an effective interaction. Test calculations with different types of CV showed that the coordination numbers, as defined by eq 6, are superior to simple interatomic distances or bond angles. The coordination number does not bias the interaction to one specific neighbor and, therefore, prejudices the reaction path to a much lower extent.

Results and Discussion

Brucite Surface Energy and Brucite−Magnesite Interface. *Surface Energy of Brucite.* The brucite structure belongs to the $P\bar{3}m1$ space group. Its lattice parameters are $a = b = 3.147$ Å and $c = 4.769$ Å. The stacking along the (0001) axis is given by one hexagonal ordered Mg layer between two hydroxyl layers (Figure 1a). The O atoms are located at ($^1/_3$, $^2/_3$, $^1/_4$) and ($^2/_3$, $^1/_3$, $-^1/_4$), and each of them has three neighboring Mg sites. The Mg atoms are, instead, 6-coordinated. Each OH faces three oppositely oriented OH groups from the neighboring (0001) layer, in an antiferromagnetic arrangement. The hydroxyl layers interact through relatively weak hydrogen bonds. Because of these weak interlayer interactions, the OH-terminated, (0001) crystallographic plane is the most common cleavage plane.

Since the dehydrogenation and the carbonation reactions occur at the surface of the brucite particles, the first step in our work is to determine which are the planes exposed by the crystallites. From the analysis of the crystalline structure, it is clear that the (0001), (1$\bar{1}$00), and (11$\bar{2}$0) surfaces are the most probable cleavage planes. For this purpose we calculate the surface energies and determine the equilibrium conformation of the crystal by Wulf construction.[19]

We model the (0001) surface with a slab in a hexagonal supercell containing 24 Mg(OH)$_2$ molecules. Since the (0001) layers are held together by weak, dispersive forces (Figure 1a), which are not well described by the DFT formalism, a fully unconstrained optimization causes an over-large outward relaxation of the ionic coordinates, resulting in a negative surface

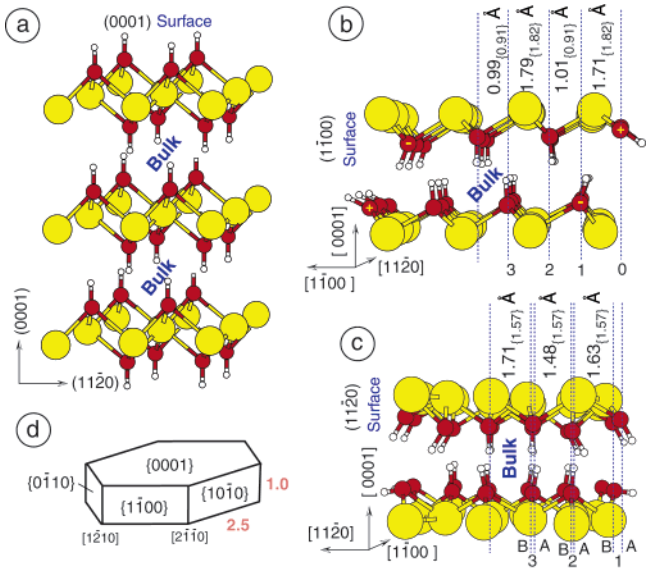

Figure 1. Pseudo 3D projections of the surface relaxation on (0001) (a), (1$\bar{1}$00) (b), and (11$\bar{2}$0) (c) faces of brucite. The yellow spheres are Mg atoms, the red ones are O atoms, and the white ones are H atoms. The dotted lines indicate the atomic planes formed by oxygen atoms. The calculated interatomic distances in the relaxed surfaces are compared with equilibrium values in the bulk, given in the curly brackets. Additional geometric parameters are summarized in Table 1. In (b), the symbols "+" and "−" are assigned to the oxygen atoms situated above and below the outermost (1$\bar{1}$00) plane of magnesium atoms, respectively. (d) Equilibrium shape of brucite crystal obtained by Wulf's method. Red numbers indicate relative size of the crystal edges.

TABLE 1: Calculated Surface Energy of Brucite

surface	(0001)	(1$\bar{1}$00)	(11$\bar{2}$0)
E_{surf} [meV/Å^2]	3.3	14.0	28.5

energy. To avoid this unphysical effect, we fix the Mg−Mg interlayer distance in the c direction. Under this constraint, the only effect of the relaxing structure is the shortening of O−H distances in the outermost atomic layer by ∼1%. The final surface energy is only 3 meV/Å^2. This is probably an underestimate since the van der Waals forces are not properly accounted for.

For the (1$\bar{1}$00) surface, we take a slab in an orthorhombic supercell of 24 Mg(OH)$_2$ molecules. The 2D lattice is rectangular, and the Mg are placed at its corners. The unit cell area is $A = (3a \times 2c)$. The Mg atoms at the surface are only 5-coordinated; i.e., there is one dangling bond per unit cell. The optimization causes the rotation of the exposed OH groups, which in the bulk lie along the c axis (compare parts a and b of Figure 1). Moreover, the interlayer distance between the first and second hydroxyl layers is reduced by 6%, as shown in Figure 1b. Table 2 reports the OH orientation, the average hydroxyl interlayer distances, and the average O−H bond lengths, as calculated for the first four hydroxyl layers. The surface energy of the relaxed structure is 14 meV/Å^2.

For the (1$\bar{1}$00) surface, the slab is an orthogonal supercell containing 24 Mg(OH)$_2$ molecules. The surface unit cell is monoclinic, with Mg atoms at its corners, and unit area $A = (2a\sqrt{3} \times 2c)$. The surface Mg atoms are only 4-coordinated; i.e., there are two dangling bonds per unit cell. The resulting strong inward attraction causes a 23% reduction of the interlayer distance between the first and second Mg layers. Also in this case, the OH at the surface change orientation and rotate outward (Figure 3c). In addition, we observe the splitting of the O atoms

TABLE 2: Average Structural Features Calculated in the First Four Planes of the (1$\bar{1}$00) Slab, after the Optimization of the Atomic Positions[a]

atomic layer	OH ∠ [11$\bar{2}$0]	OH ∠ [1$\bar{1}$00]	OH ∠ [0001]	*d*(OO) [Å]	*d*(OH) [Å]
1	90	35	55	1.71 {1.82}	0.97 {0.98}
2	90	74	164	1.01 {0.91}	0.99 {0.98}
3	90	87	6	1.79 {1.82}	0.98 {0.98}
4	90	89	177	0.99 {0.91}	0.98 {0.98}

[a] The angles of the OH bonds with respect to the three main axes are reported in the second, third, and fourth columns. The corresponding values in the bulk are 90°, 90°, and 0° (or 180° depending on the orientation), respectively. In the fifth column the O−O interlayer distances are reported, with respect to the next, lower layer.The O−H bond lengths are reported in the last column. The values in curly brackets are the equilibrium distances in the bulk. See also Figure 1b.

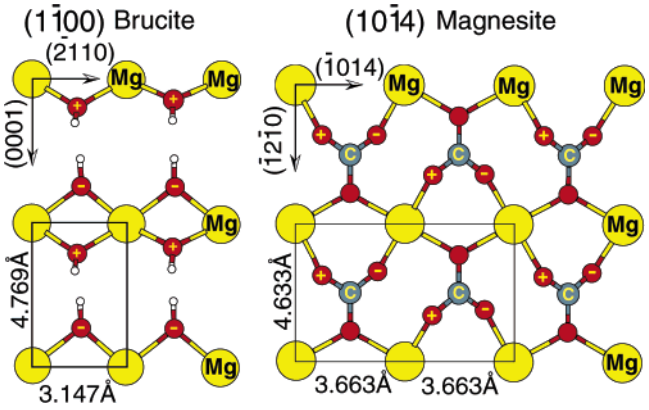

Figure 2. Top view of the optimized (1$\bar{1}$00) surface of brucite and (10$\bar{1}$4) cleavage plane of magnesite. The oxygen atoms, situated respectively above and below the outermost plane of magnesium atoms, are indicated by "+" and "−" (see also Figure 1b). The remaining O atoms in the magnesite structure are situated within the (10$\bar{1}$4) plane formed by magnesium atoms.

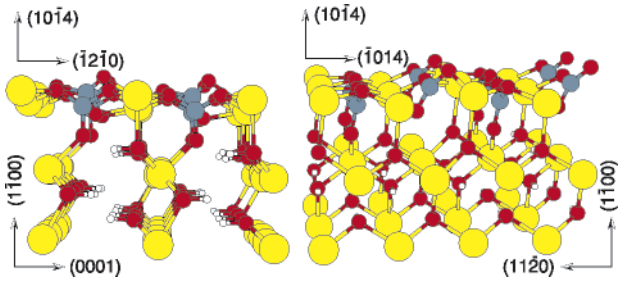

Figure 3. Film of magnesium carbonate on (1$\bar{1}$00) surface of brucite, as obtained by geometry optimization.

into two sublattices. Table 3 reports the average orientation of the OH, the O−H bond lengths, and the first three interlayer distances between the Mg layers.

By using the Wulf construction and the calculated surface energies, we find that the $T = 0$ equilibrium shape of a brucite crystal is a hexagonal prism with (0001) and (1$\bar{1}$00) faces (Figure 1d). This is in agreement with previous work[15] and with the shape experimentally determined by transmission electron microscopy and X-ray diffraction.[20]

Brucite−Magnesite Interface. The mechanism that drives the dehydroxylation of $Mg(OH)_2$ is the interlayer diffusion of protons and hydroxyl groups with the final formation and release of water molecules at the surface. Since the (0001) slab terminates with Mg atoms, it is quite unlikely that the process occurs through this surface, though it is definitely the most favorable cleavage plane.

TABLE 3: Average Structural Features Calculated in the First Three Planes of the [11$\bar{2}$0] Slab, after the Optimization of the Atomic Positions[a]

atomic layer	OH ∠ [11$\bar{2}$0]	OH ∠ [1$\bar{1}$00]	OH ∠ [0001]	*d*(OH) [Å]	*d*(Mg−Mg) [Å]
1 A	63	107	148	0.97	1.23 {1.57}
1 B	39	53	98	0.98	
2 A	63	79	151	0.99	1.75 {1.57}
2 B	85	81	10	0.98	
3 A	84	96	8	0.98	1.48 {1.57}
3 B	89	90	178	0.98	

[a] Because of the splitting of the O layers into two sublayers, A and B, two sets of values are reported for the angles between the OH bond and the three main axes and for the OH distances. The angles are in the second, third, and fourth columns. The corresponding values in the bulk are 90°, 90°, and 0° (or 180° depending on the orientation), respectively. The O−H bond lengths are reported in the fifth column, and the Mg interlayer distances are in the last one. See also Figure 1c.

On the other hand, the presence of channels along the (1$\bar{1}$00) axis suggests that the H and OH species can easily access the (1$\bar{1}$00) surface, where they can react with other O and H atoms and be released as water molecules. Therefore, from now on, we assume that the reactive surface must be the (1$\bar{1}$00). A further argument in favor of this choice is its compatibility with the (10$\bar{1}$4) plane of magnesite. As already mentioned in the Introduction, the magnesite crystal grows along the (10$\bar{1}$4) axis. Success of this process is obviously dependent on the characteristic structure of the substrate, i.e., brucite.

Comparing the structure of the (1$\bar{1}$00) brucite surface and the (10$\bar{1}$4) magnesite surface, we observe that both have a rectangular Mg sublattice. The unit cell areas are 3.147 × 4.769 Å^2 and 3.663 × 4.633 Å^2, respectively. Therefore, the cell size mismatch produces a 14% difference in the Mg−Mg nearest-neighbor distances, whereas the second neighbors' distances are practically unaffected. This suggests possible epitaxial growth of the magnesite on the (1$\bar{1}$00) surface of brucite. To verify the stability of the brucite/magnesite interface, we construct a magnesite layer on top of the (1$\bar{1}$00) brucite slab, equilibrate the atomic positions by a slow thermal annealing, and finally observe it in a MD run at 300 K. During the heating, the magnesite layer is slightly distorted, as shown in Figure 3. The Mg atoms along the (10$\bar{1}$4) axis are alternately displaced up and down with respect to their original positions. The $[CO_3]^{2+}$ groups, on the other hand, sink deeper into the brucite structure. Nevertheless, the $MgCO_3$ film maintains its main features, and we can reasonably conclude that the epitaxial growth of a thicker magnesite film from the (1$\bar{1}$00) surface of brucite is possible.

Dehydroxylation and Carbonation on (1$\bar{1}$00) Surface of Brucite. The formation of the magnesite layer from brucite is a complex process that is most probably obtained through a series of sequentially activated events. For the sake of clarity and simplicity, we focus our attention on the two main steps separately.

First we study the mechanism of the dehydroxylation reaction on the (1$\bar{1}$00) brucite surface. Since we are interested in the atomic rearrangements at the surface, we ignore the interactions with the external fluid. However one should not forget that these interactions are important to determine the correct rate of the reaction, as well as for the thermodynamic stability of the dehydrated surface.

Once the OH vacancy is formed at the (1$\bar{1}$00) surface, we assume the presence of a CO_2 molecule in the vicinity and study the adsorption process. Also in this case, we do not take into account a realistic fluid, but simply add one CO_2 molecule close to the vacant site to facilitate the reaction.

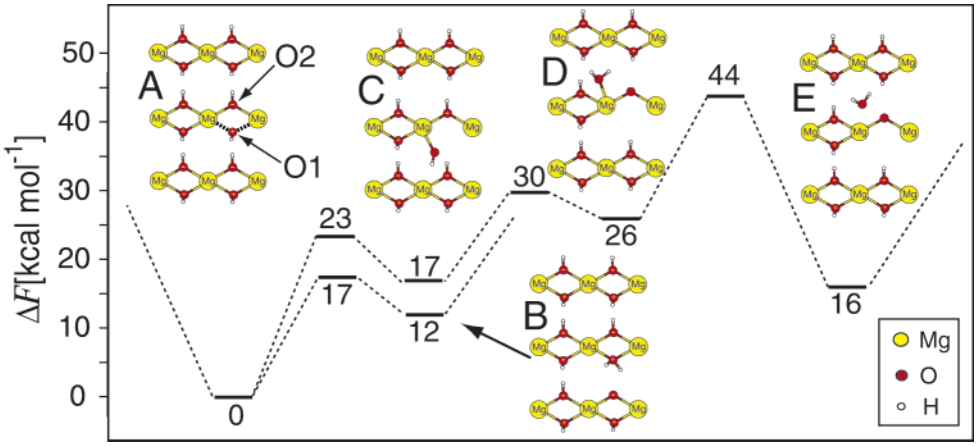

Figure 4. Estimation of the free energy profile for dehydration reaction on $(1\bar{1}00)$ surface of brucite observed applying the metadynamics technique. The three CV used for metadynamics are the coordination numbers of O1 with respect to the two nearest Mg atoms, connected to O1 by bold-dashed lines (panel A), and the coordination number of the same O1 with respect to all H atoms. As described in the text, we observe first unsuccessful path from A to B. Afterward, the system goes back to A and follows the ACDE path. The energy values indicated along the path are the barriers and relative energies of the encountered intermediates, calculated with the eq 5. The errors of the free energy profile are estimated within 2−5 kcal/mol.

In both cases, we apply the metadynamics methodology to determine and characterize the most probable reaction pathways.

Dehydroxylation on $(1\bar{1}00)$ Surface. We pick up one O atom at the surface (they are all equivalent) and take its coordination with respect to its two nearest Mg neighbors as the first two CV (in eq 4 $N_J = 1$ and $R_0 = 3.0$ Å). The third CV is the coordination of the same O, with respect to all the H of the system ($R_0 = 1.6$ Å).

The contributions of the hills to the time-dependent potential V are 0.45 kcal/mol high, whereas their width is on average 0.05. The force constants are 2 hartrees for the first two CV and 1.5 hartrees for the third, and the fictitious masses are 50 and 40 amu, respectively.

During the metadynamics, the system passes through a chain of intermediate states and crosses several barriers of the order of 20 kcal/mol. Figure 4 shows a schematic summary of the main steps along the metadynamics trajectory. The reported values of the free energy levels, relative to the initial configuration A, are estimated to be within an error of a few (2−5) kcal/mol.

According to the observed pathway, the easiest way for the oxygen O(1), in state A, to acquire a second proton is to take it from the closest $Mg(OH)_2$ layer. Since the O at the surface are under coordinated, O(1) can saturate its charge by the acquisition of one proton. The activation barrier for this reaction (A to B in Figure 4) is, indeed, only 17 kcal/mol, and the B state is only 12 kcal/mol more energetic than A. However, the complete dehydroxylation is not likely to proceed from this point, since the H_2O formed is trapped within the Mg plane, due to the electrostatic interactions with the bare O^- on the opposite layer. The Mg−O(1) bonds in the B configuration are only slightly elongated. Since the B to A transition state is only 5 kcal/mol above the bottom of the B well, it is more convenient to go back to the initial state rather than to break the Mg−O bonds and release the water molecule. Once the two basins are filled at least up to the A to B transition state, the trajectory can fluctuate freely in the CV space between the two states, without crossing.

The successful reaction path is obtained by filling the well up to the second transition state, which is at 23 kcal/mol from the bottom of A and connects A to a new basin of attraction that we name C in Figure 4. In state C, one of the two Mg−O bonds is broken, and the resulting $(OH)^-$ is free to rotate around the still bonded Mg until it acquires an almost vertical position over the surface. From this position, the $(OH)^-$ is able to grab a second proton from the opposite O(2), which is ionically bonded to the same Mg (Figure 4D). The barrier corresponding to the proton exchange is only 13 kcal/mol. Actually, the partial dissociation of O(1)H leaves an excess of positive charge on the Mg ions, the remaining electrostatic Mg−O(2) interactions become stronger, and for this reason the release of the proton from O(2) is favored.

The successful mechanism involves two intermediate configurations and three energy barriers. The rate-limiting step is the first Mg−O(1) bond-breaking (∼20 kcal/mol), whereas the total activation energy is estimated at ∼44 kcal/mol, within an error of 2−5 kcal/mol. The widespread of the experimentally reported values, 13−58 kcal/mol,[5] is in agreement with our estimation.

The observed reaction path is characteristic of a rough and complex free energy surface, with a high density of saddle points and local minima, where the optimal sequence of states to the final products is not always uniquely determined.

We remark that we overestimate the energy of the final state because we neglect the interactions with the realistic environment. The study of the influence on the reaction rates of thermodynamic quantities like the water activity and partial pressures in the fluid is beyond the purposes of this work.

Carbonation of Partly Dehydrated $(1\bar{1}00)$ Surface of Brucite. The creation of the OH vacancy on the $(1\bar{1}00)$ surface leaves two under-coordinated Mg ions and additional dangling bonds, which can be saturated by the adsorption of the CO_2 molecule. On the other hand, it is not clear how the CO_2 may be accommodated on the surface and what is the role of the deprotonated O(2) in the process.

Once more, the metadynamics proved capable of unveiling the details of this process. We use three coordination numbers as CV. The first is the coordination of the oxygen atom in CO_2 molecule with respect to one under-coordinated Mg site ($R_0 =$ 2.4 Å), which is also useful in order to encourage the interaction of the CO_2 with the surface and keep it close in the initial stage of the simulation. The next CV is the coordination of one of the two O atoms in CO_2 with respect to all the Mg ($R_0 = 2.4$ Å). The last CV is the coordination of the C atom with respect to all the oxygen atoms ($R_0 = 1.6$ Å). This latter CV is chosen so as not to bias the formation of the $[CO_3]^{2+}$complex by forcing

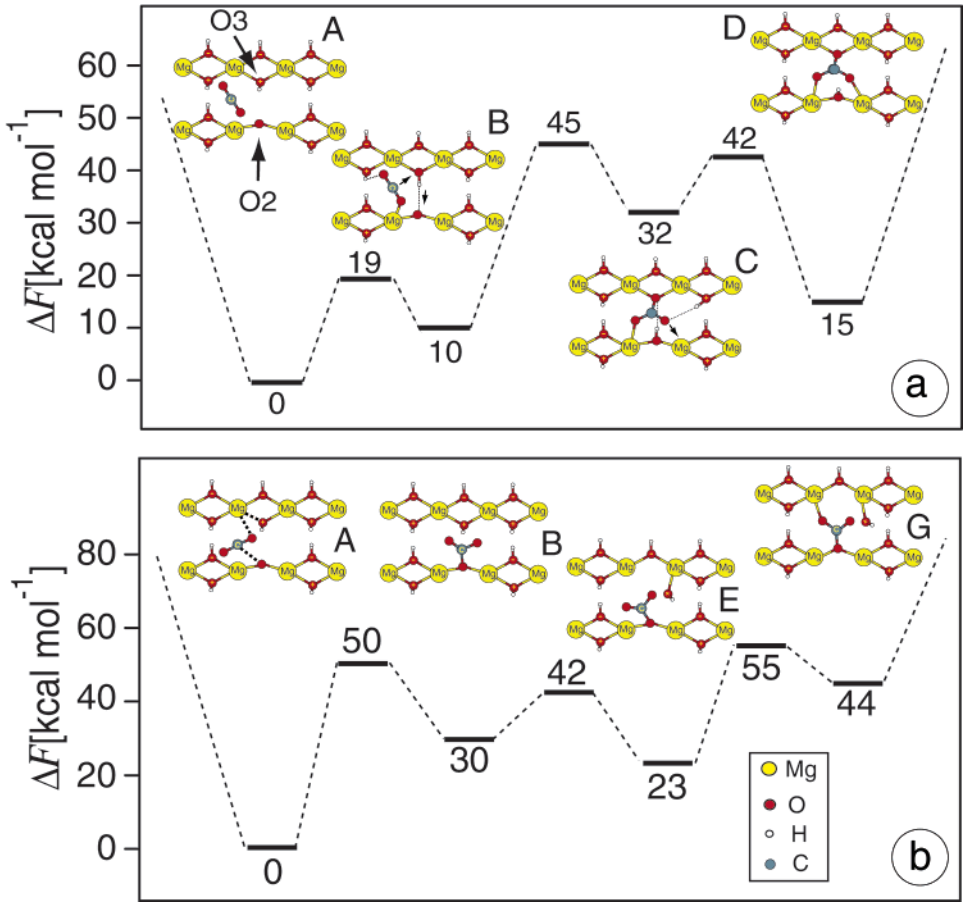

Figure 5. Estimation of the free energy profile for the carbonation reaction on the partly dehydrated ($1\bar{1}00$) surface of brucite observed applying the metadynamics technique. The energy values indicated along the path are the barriers and relative energies of the encountered intermediates, calculated with the eq 5. The errors of the free energy profile are estimated within 2−5 kcal/mol. Two sets of CV have been used to observe different reaction pathways. (a) The CV are the coordination number of one O atom in CO_2 molecule with respect to the one under-coordinated Mg site, the coordination of the second O atom in CO_2 molecule with respect to all Mg atoms, and the coordination of carbon with respect to all oxygens. (b) The CV, indicated by bold dotted lines (panel A), are coordination number of O in CO_2 molecule with respect to one under-coordinated Mg atom, the coordination of the O atom on brucite surface with the same Mg atom, and coordination of the carbon with respect to the under-coordinated oxygen on brucite surface.

the C interaction to some predefined O atom. We use the same force constants (1.8 hartrees) and masses (50 amu) for all the CV. To build up the V potential, we add hills 0.63 kcal/mol high and 0.07 arbitrary units wide.

The metadynamics is started from configuration A, shown in Figure 5a. The first reaction process that is activated is the partial adsorption of the CO_2 molecule at the under-coordinated Mg site. The positive charge on the Mg ion attracts one O of the CO_2, and by crossing a small activation barrier of 19 kcal/mol, a Mg−O ionic bond is formed (Figure 5a B). Because of the activated Mg−O interaction, the charge distribution of the CO_2 molecule is slightly modified, and the C atom can more easily accept a third O. The third C−O bond is formed with the protonated O(3), which sits in the opposite (0001) layer, and the system moves to the C state in Figure 5a. For the formation of this bond a proton transfer from O(3) to O(2) is required. The two events, the C−O bond formation and the proton transfer, occur simultaneously, in a concerted fashion, and the entire process from B to C requires an activation energy of 35 kcal/mol. The final stabilization of the CO_3 complex is obtained by the formation of the second Mg−O bond and the rearrangement of the O(2)H group, which sinks deeper into the brucite structure. The rate-limiting step of the carbonation mechanism turns out to be the C−O bond formation, i.e., the sp^3 hybridization of the C atom.

We have also considered an alternative mechanism for the carbonation in which the CO_2 interacts directly with one 5-coordinated Mg ion. In this case the formation of the CO_3 complex competes with the Mg−OH bonds present and can occur only if a partial dehydroxylation of the surface is induced.

For the study of this mechanism, the metadynamics is started from the same configuration A as the one used as initial state in the previous simulation, but obviously we use different CV. The first one is the coordination of the C atom with respect to the deprotonated O(2), the second is the coordination of the CO_2 to one of the 5-coordinated Mg ions, and the last CV is the coordination of one OH group with the same Mg atom (Figure 5b A). The force constants are equal to 2.0 hartrees, and masses equal 50 amu for all the CV. The hills contributing to the potential V are 0.45 kcal/mol high and their width is 0.05 arbitrary units. The pathway that we observe is displayed schematically in Figure 5b. First the C atom is attracted by the deprotonated O(2). The CO bond is formed by crossing a barrier of ∼50 kcal/mol. This value is comparable to the sum of the barriers (19 + 35 kcal/mol) of the first two steps in the carbonation reaction described in the previous paragraph (see Figure 5a). The interactions between the oxygen atoms of the just formed [CO_3] complex and the Mg ions eventually induce the OH to break one Mg−O bond. The partially dissociated OH fluctuates over the surface and visits several intermediate

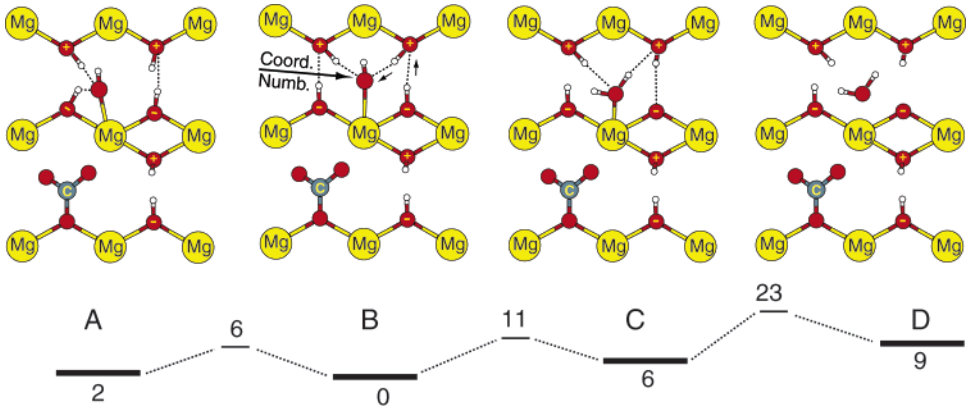

Figure 6. Estimation of the free energy profile for the dehydration−carbonation reaction induced by the presence of an adsorbed $[CO_3]^{2+}$ complex. The reaction mechanism is described by means of the coordination number of oxygen atom indicated in the panel B, with respect to all hydrogen and magnesium atoms. The energy values indicated along the path are the barriers and relative energies of the encountered intermediates, calculated with the eq 5 (kcal/mol). The errors of the free energy profile are estimated within 2−5 kcal/mol.

states, which are all similar and separated by low-energy barriers (Figure 5b, D, E, G). In the final configuration, the OH is vertical over the surface plane, as in the intermediate C along the dehydroxylation path (Figure 4). Although in this process the dehydroxylation is not complete, it shows a possible mechanism in which the carbonation and dehydroxylation processes cooperate in the surface reconstruction.

To complete the dehydroxylation, the OH should find a second proton and leave the surface as H_2O. Therefore, we start a new metadynamics run from the last configuration obtained in the carbonation process reported in Figure 5b. The two CV are the coordination numbers of the oxygen of the displaced OH, with respect to the Mg and to the H species, with R_0 set at 2.9 and 1.6 Å, respectively. The force constants and the masses are 1.9 hartrees and 55 amu for the first CV and 1.4 hartrees and 45 amu for the second, whereas the height of the hills is 0.43 kcal/mol and their width 0.05 arbitrary units. As expected, the energy barriers involved in this process are quite small. The OH changes its position several times, while the system visits different intermediates. These states are stabilized by the formation of H bonds between the O atom of the OH and other H atoms on the surface. Some of them are shown in Figure 6, together with the activation energies required to cross the small separating barriers. The final formation of the water molecule occurs with a concerted, double proton transfer. The OH acquires one proton from the opposite (0001) layer, and simultaneously the deprotonated O accepts one proton from the opposite OH (Figure 6B,C). In the final step the Mg−O bond is broken by crossing a barrier of 17 kcal/mol. Also by following this alternative path, the dissociation of the O from the Mg atoms is the rate-limiting step of the entire process.

Conclusions

We have studied the dehydroxylation and carbonation processes at the $(1\bar{1}00)$ brucite surface, which are expected to be the basic processes for the formation of a magnesite layer on a brucite substrate. The choice of the $(1\bar{1}00)$ surface is motivated by the fact that it is one of the most common cleavage planes of brucite and, in addition, is structurally similar to the preferred cleavage plane of magnesite.

To our knowledge, very little is to be found in the literature about the atomistic rearrangements that might be responsible for these processes. In our study, we have looked at several different mechanisms. First we have considered separately dehydroxylation and the carbonation on a partly dehydroxylated surface. In the last part of our work, we have studied how the adsorption of CO_2 can induce the formation of defects at the surface and the consequent release of water.

We notice that, in dehydroxylation, the rate-limiting reaction is the Mg−O bond breaking, whereas in carbonation, it is the sp^3 hybridization of the C atom. The easy proton transfers and the mobility of the OH, in the region between the two opposite hydroxyl layers, play a crucial role. We suggest that the same (0001) interlayer space may be used to supply, from the bulk, additional OH and protons to the surface. This would create the conditions for further water formation, leaving, at the same time, an increasing number of vacant sites in the brucite structure.

As expected, the partial dehydroxylation of the brucite surface is a necessary precursor for the carbonation reaction. Once the surface is dehydroxylated, the activation energy for CO_2 adsorption at some under-coordinated Mg ion plus $[CO_3]^{2+}$ formation is about 45 kcal/mol. On the other hand, from our simulations we observe that the carbonation process itself can induce further dehydroxylation, and the total costs would be comparable to the sum of the activation energies of separate dehydroxylation and carbonation events. Obviously, the complete surface saturation, by $[CO_3]^{2+}$ complexes, prevents further dehydroxylation from taking place, as was observed in numerous experimental studies.[6,8] The same investigations indicate, however, that complex morphological reconstruction of the brucite matrix might create new highly reactive sites, despite the passivating layer of carbonate. Therefore, a detailed study of translamellar cracking, delamination, and diffusion of water in bulk brucite would complete the picture of the solid-state transformation of brucite into magnesite by CO_2 adsorption.

Acknowledgment. The authors are grateful to Prof. Marco Bernasconi and Dr. Alessandro Laio for fruitful discussions. Special thanks go to Jean Favre and Mario Valle for help in visualizing the results. We appreciate careful consideration of the manuscript by reviewers, whose comments helped us to improve the final version of the manuscript.

References and Notes

(1) Laio, A.; Parrinello, M. *Proc. Natl. Acad. Sci. U.S.A.* **2002**, *99*, 12562−12566.
(2) Iannuzzi, M.; Laio, A.; Parrinello, M. *Phys. Rev. Lett.* **2003**, *90*, art. no. 238302.
(3) Seifritz, W. *Nature (London)* **1990**, *345*, 486.
(4) Lackner, K. S.; Wendt, C. H.; Darryl, P.; Butt, D. P.; Joyce, E. L., Jr.; Sharp, D. H. *Energy* **1995**, *20*, 1153−1170.

(5) Butt, D. P.; Lackner, K. S.; Wendt, C. H.; Conzone, S. D.; Kung, H.; Lu, Y.-C.; Bremser, J. K. *J. Am. Ceram. Soc.* **1996**, *79*, 1892−1898.

(6) Bearat, H.; McKelvy, M. J.; Chizmeshya, A. V. G.; Sharma, R.; Carpenter, R. W. *J. Am. Ceram. Soc.* **2002**, *85*, 742−748.

(7) McKelvy, M. J.; Sharma, R.; Chizmeshya, A. V. G.; Carpenter, R. W.; Streib, K. *Chem. Mater.* **2001**, *13*, 921−926.

(8) (a) Gordon, R. S.; Kingery, W. D. *J. Am. Ceram. Soc.* **1966**, *49*, 12. (b) Halikia, I.; Neou-Syngouna, P.; Kolitsa, D. *Thermochim. Acta* **1998**, *320*, 77−88. (c) Kim, M. G.; Dahmen, U.; Searcy, A. W. *J. Am. Ceram. Soc.* **1987**, *70*, 146−154. (d) Kim, M. G.; Dahmen, U.; Searcy, A. W. *J. Am. Ceram. Soc.* **1988**, *71*, C373−C375. (e) Laureiro, Y.; Jerez, A.; Pico, C.; Veiga, M. L. *Thermochim. Acta* **1991**, *182*, 47−56. (f) Moodie, A. F.; Warble, C. E. *J. Cryst. Growth* **1986**, *74*, 89−100.

(9) Chizmeshya, A. V. G.; McKelvy, M. J.; Sharma, R.; Carpenter, R. W.; Bearat, H. *Mater. Chem. Phys.* **2003**, *77*, 416−425.

(10) (a) Higgins, S. R.; Boram, L. H.; Eggleston, C. N.; Coles, B. A.; Compton, R. G.; Knauss, K. G. *J. Phys. Chem. B* **2002**, *106*, 6696−6705. (b) Jordan, G.; Higgins, S. R.; Eggleston, C. M.; Knauss, K. G.; Schmahl, W. W. *Geochim. Cosmochim. Acta* **2001**, *65*, 4257−4266.

(11) Car, R.; Parrinello, M. *Phys. Rev. Lett.* **1985**, *55*, 2471−2474.

(12) Kohn, W.; Sham, L. J. *Phys. Rev.* **1965**, *140*, A1133−A1138.

(13) (a) Becke, A. D. *Phys. Rev. A* **1988**, *38*, 3098−3100. (b) Lee, C.; Yang, W.; Parr, G. M. *Phys. Rev. B* **1988**, *37*, 785−789.

(14) Troullier, N.; Martin, J. L. *Phys. Rev. B* **1991**, *43*, 1993−2006.

(15) Masini, P.; Bernasconi, M. *J. Phys.: Condens. Matter* **2001**, *13*, 1−12.

(16) Raugei, S.; Silvestrelli, P. L.; Parrinello, M. *Phys. Rev. Lett.* **1999**, *83*, 2222−2225.

(17) Carter, E. A.; Ciccotti, G.; Hynes, J. T.; Kapral, R. *Chem. Phys. Lett.* **1989**, *156*, 472−477.

(18) (a) Gervasio, F.; Iannuzzi, M.; Laio, A.; Parrinello, M. *Chem.—Eur. J.*, submitted. (b) Stirling, A.; Iannuzzi, M.; Laio, A.; Parrinello, M. *ChemPhysChem.*, in press.

(19) Zangwill, A. *Physics at Surfaces*; Cambridge University Press: New York, 1988; p 454.

(20) Carrott M. R.; Carrott, P.; de Carvalho, M. B.; Sing, K. S. W. *J. Chem. Soc., Faraday Trans.* **1991**, *87*, 185−191.